Nonlinear effects of phase modulation in an electron storage ring

J. M. Byrd,[1] W.-H. Cheng,[2] and F. Zimmermann[3]
[1]*Lawrence Berkeley National Laboratory, One Cyclotron Road, Berkeley, California 94720*
[2]*Department of Physics, University of California Berkeley, Berkeley, California 94720*
[3]*Stanford Linear Accelerator Center, Stanford, California 94309*
(Received 14 July 1997; revised manuscript received 4 November 1997)

We present results of experimental studies of the nonlinear dynamics of synchrotron oscillations in the presence of phase modulation in an electron storage ring. A streak camera is used to observe the longitudinal distribution of an electron bunch directly as it forms two stable resonant islands. The positions of the fixed points as a function of modulation frequency agree well with theory. We also present measurements of the diffusion rate from one stable island to the other for a fixed modulation frequency, which show agreement with the diffusion rates expected from large-angle intrabeam (Touschek) scattering. These results also explain anomalous results of beam transfer function diagnostic measurements obtained at other electron storage rings. [S1063-651X(98)01604-3]

PACS number(s): 41.85.−p, 41.75.Ht, 29.27.Fh, 07.85.Qe

I. INTRODUCTION

The longitudinal charge density of an electron bunch is a fundamental parameter in storage ring operation. In collider rings, maximum luminosity is reached when the bunch length is adjusted to be approximately equal to the minimum vertical β function at the interaction point. In a synchrotron light source the bunch length determines the time structure of the radiation. The equilibrium longitudinal phase space distribution in an electron storage ring is determined by a combination of different factors. Neglecting instabilities, the energy spread results from a balance between radiation damping and excitation from synchrotron radiation and intrabeam scattering. The longitudinal focussing potential, usually from the main radio-frequency (rf) accelerating system, determines the corresponding longitudinal charge density. Because the accelerating rf voltage is typically sinusoidal, the resulting potential, in which electrons oscillate, gives rise to nonlinear synchrotron motion. The nonlinear motion has a dramatic impact on the longitudinal charge distribution in the presence of both single and multibunch coherent beam instabilities [1,2] and random or periodic external modulations of the rf voltage. As performance demands increase on beam intensity, lifetime, and reductions in bunch length, it is becoming increasingly important to understand the nonlinear longitudinal effects in electron rings.

Nonlinear synchrotron oscillations in hadron accelerators have been studied experimentally in the past [3–6]. In this paper, we present an experimental study of nonlinear longitudinal dynamics with phase modulation in an electron storage ring with measurements performed at the Advanced Light Source (ALS) located at Lawrence Berkeley National Laboratory. Using a dual axis streak camera, the effect of the nonlinear dynamics of single electrons can be directly observed on the longitudinal distribution of the entire electron bunch as the electrons populate the stable fixed points of the system. The stable fixed points as viewed on the streak camera are mapped as a function of modulation frequency and compared with calculated values. Real time diffusion is observed from one stable island to the other, and the measured rate is compared with the rate expected from large-angle intrabeam scattering. As an aside, we use these results to explain an anomalous effect of the nonlinear motion on a common diagnostic measurement technique, the longitudinal beam transfer function.

Section II summarizes a Hamiltonian formulation of the longitudinal dynamics and describes the calculation of the diffusion between stable fixed points. Section III presents measurements of the longitudinal response as a function of modulation frequency, the diffusion rate between islands, and the effect on longitudinal beam transfer function measurements. Section IV provides a discussion and summary.

II. SYNCHROTRON OSCILLATIONS WITH PHASE MODULATION

A. Single particle dynamics

In this section, we present a summary of the Hamiltonian formulation following Ref. [4]. The equations of motion for an electron can be written as

$$\varphi' = h\eta\delta + \varphi_m \nu_m \cos\ \nu_m \theta, \tag{1}$$

$$\delta' = \frac{e\hat{V}}{2\pi E_0}[\sin(\varphi+\phi_s) - \sin\ \phi_s] - \lambda\delta, \tag{2}$$

where the rf phase is modulated as $\varphi_{\mathrm{mod}} = \varphi_m \sin\ \nu_m\theta$, φ_m is the amplitude of the rf phase modulation, $\nu_m = f_m T_0$ is the tune of the rf phase modulation, T_0 is the revolution period, $\varphi = \phi - \phi_s$ is the particle's phase relative to the synchronous phase ϕ_s, $\delta = (p-p_0)/p_0$ is the particle's momentum relative to the synchronous momentum $p_0' = d/d\theta$, $\theta = 2\pi n$, n is the number of revolution, h is the harmonic number, η is the slip factor, $\hat{V}$ is the peak rf voltage, E_0 is particle's energy, λ is the radiation damping rate, and U_0 is the energy loss per turn. Ignoring damping, the Hamiltonian for this system can be written as

$$\widetilde{H} = \frac{h\eta}{\nu_{s0}} H = \frac{\nu_{s0}}{2}\widetilde{\delta}^2 + \varphi_m \nu_m \widetilde{\delta}\ \cos\ \nu_m\theta + \nu_{s0}[1 - \cos\ \varphi + (\sin\ \varphi - \varphi)\tan\ \phi_s]. \tag{3}$$

The synchrotron tune is $\nu_{s0}=(-h\eta e\hat{V}\cos\phi_s/2\pi E_0)^{1/2}$, and $\tilde{\delta}=(h\eta/\nu_{s0})\delta$.

Near a resonance ($\nu_m\approx\nu_{s0}$), it is most useful to examine the averaged Hamiltonian in a coordinate frame with the phase relative to the modulated phase, and rotating at the modulation frequency. This can be done via a series of canonical transformations for the Hamiltonian, including the nonzero synchronous phase, which leads to the averaged Hamiltonian expressed in action-angle coordinates

$$\mathcal{H}=1-\mathcal{J}_0(\varphi_m)\mathcal{J}_0(\sqrt{2I})+(\tfrac{1}{2}-\nu)I - 2\mathcal{J}_1(\varphi_m)\mathcal{J}_1(\sqrt{2I})\cos\Phi, \quad (4)$$

where $\sqrt{2J}\cos\Phi=(\varphi-\varphi_m\sin\nu_m\theta-\nu_m\theta)$, $\sqrt{2J}\sin\Phi=-\tilde{\delta}$, and $\nu=\nu_m/\nu_{s0}$. The resonant system of Eq. (4) can be approximated by the expansions of the Bessel functions for I,

$$\mathcal{J}_0(\sqrt{2I})\approx 1-\frac{I}{2}+\frac{I^2}{16} \quad \text{and} \quad \mathcal{J}_m(\sqrt{2I})\approx\frac{(I/2)^{m/2}}{m!}, \quad (5)$$

and by assuming a small amplitude of the phase modulation, i.e., $\varphi_m\ll 1$, where $\mathcal{J}_0(\varphi_m)\approx 1$, and $\mathcal{J}_1(\varphi_m)\approx\varphi_m/2$. The Hamiltonian of the primary resonance becomes

$$\mathcal{H}\approx(1-\nu)I-\frac{I^2}{16}-\varphi_m\sqrt{\frac{I}{2}}\cos\Phi. \quad (6)$$

The expression of $\mathcal{H}$ is identical to the one obtained in Ref. [4], for the special case of $\phi_s=0$. The nonzero synchronous phase does not explicitly appear in the averaged Hamiltonian, but is implicitly expressed in ν_{s0}.

This Hamiltonian has either one or three fixed points depending on the modulation tune. Below the so-called bifurcation tune, three fixed points, given by $\bar{Q}=\pm\sqrt{2\bar{I}}$, coexist:

$$\bar{Q}_A=-\frac{8}{\sqrt{3}}\sqrt{\mu}\cos\frac{\xi}{3} \quad \text{(stable)}, \quad (7)$$

$$\bar{Q}_B=\frac{8}{\sqrt{3}}\sqrt{\mu}\sin\left(\frac{\pi}{6}-\frac{\xi}{3}\right) \quad \text{(stable)}, \quad (8)$$

$$\bar{Q}_C=\frac{8}{\sqrt{3}}\sqrt{\mu}\sin\left(\frac{\pi}{6}+\frac{\xi}{3}\right) \quad \text{(unstable)}, \quad (9)$$

where $\mu=1-\nu$, $\mu_c=1-\nu_c$, $\xi=\arctan\sqrt{(\mu/\mu_c)^3-1}$, and ν_c is the normalized bifurcation tune: $\nu_c=1-3(\phi_m/16)^{2/3}$. Note that fixed point C is unstable. Above the bifurcation tune, the fixed point is given by

$$\bar{Q}_A=-(4\phi_m)^{1/3}\left\{\left[\sqrt{1-\left(\frac{\mu}{\mu_c}\right)^3}+1\right]^{1/3} - \left[\sqrt{1-\left(\frac{\mu}{\mu_c}\right)^3}-1\right]^{1/3}\right\}. \quad (10)$$

The fixed points are shown as a function of modulation tune in the response curve in Fig. 1. The amplitudes of the separatrices are also shown. Note that the opposite signs of stable fixed points A and B indicate that, in the lab coordinate frame, the two points oscillate out of phase.

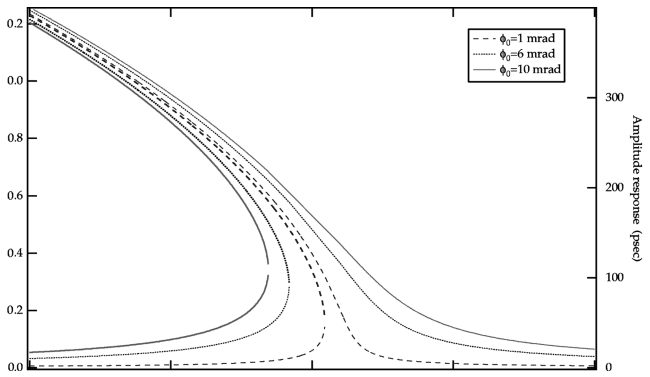

FIG. 1. Response of driven longitudinal oscillations for three excitation amplitudes. The nominal synchrotron frequency is 11.6 kHz.

A Poincaré map of the Hamiltonian in the resonant rotating reference frame for the case of three modulation frequencies is plotted in Fig. 2. In Fig. 2a, the modulation frequency is well below the bifurcation frequency and two separate stable islands appear. In Fig. 2(b), the modulation frequency is just below the bifurcation frequency, and stable area B almost disappears. Above the bifurcation frequency, only island A remains. Note that islands A and Bcorrespond to the negative and positive stable branches of the response curve shown in Fig. 1.

B. Interisland diffusion

For a distribution of electrons in phase space with finite area, it is interesting to consider diffusion of electrons from one stable island to the other. In this section we present an estimate of the diffusion rate using a modified intrabeam scattering theory. A detailed calculation of the evolution of the distribution based on a solution of the Fokker-Plank equation is beyond the scope of this paper. We considered both quantum excitation and large-angle intrabeam (Touschek) scattering as interisland diffusion mechanisms. For conditions in our studies, Touschek scattering dominates because of the relatively high bunch charge density due to the small transverse beam size except at very low beam currents. To estimate the diffusion rate, we use the approach typically used to calculate beam lifetimes due to Touschek scattering [8,9]. In this approach, the loss rate is found by integrating the probability for an electron to be scattered beyond an energy aperture, δ_{aperture}, over the distribution of electrons within the bunch. Usually the energy acceptance is taken as the acceptance of the rf bucket. For our estimate of the diffusion rate, we use the separatrix of island B as the energy acceptance and assume that all electrons are scattered from island B to island A. We consider only the initial diffusion from island B to island A and ignore any diffusion from island A to island B. Distortion of the island structure due to radiation damping and any modulation of the bunch length is ignored.

The Touschek scattering rate from island A or B, $1/\tau_{A,B}=dN_{A,B}/dt/N_{A,B}$, in the nonrelativistic approximation is given by

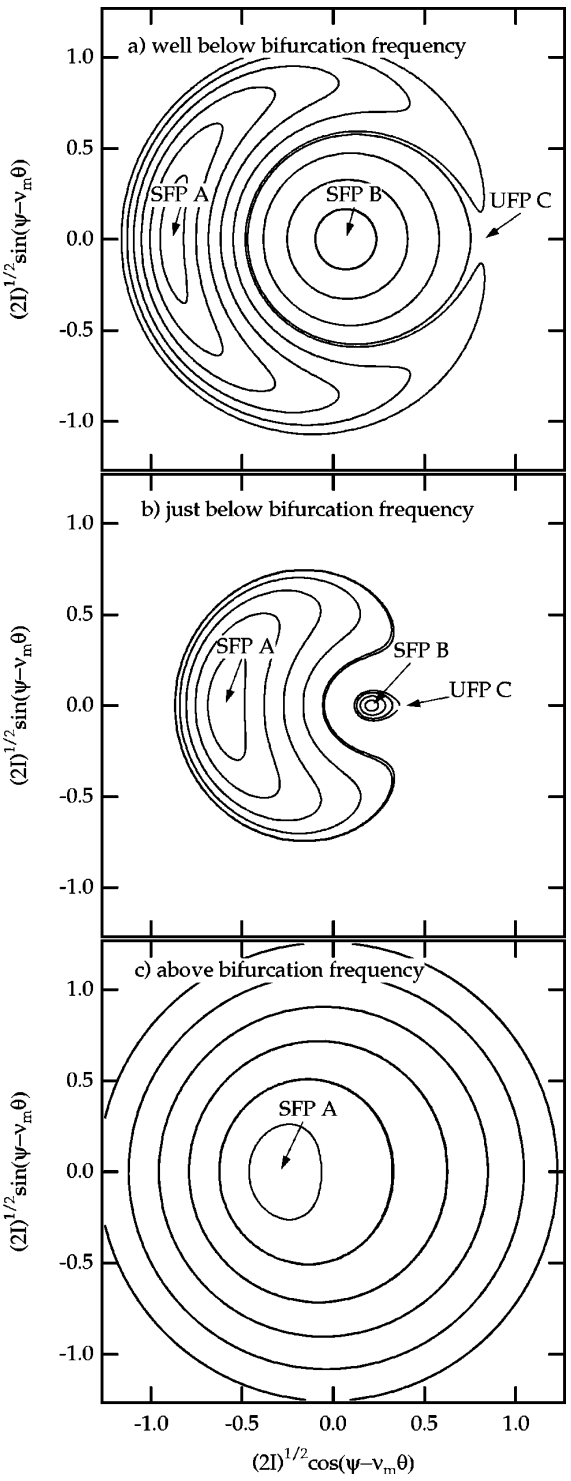

FIG. 2. Phase space diagrams in a frame rotating at the modulation frequency. The two stable fixed points are shown. (a) Modulation frequency well below the bifurcatioin frequency. (b) Just below the bifurcation frequency. (c) Above the bifurcation frequency.

$$\frac{1}{\tau_{A,B}}=\frac{1}{C}\oint ds\,\frac{\sqrt{\pi}r_e^2 cN_{A,B}F(\epsilon_{A,B})}{\delta q\,\gamma^2(\delta^m_{A,B})^2V_{A,B}}, \tag{11}$$

where the integral is over the circumference C, and r_e denotes the classical electron radius, c the speed of light, $N_{A,B}$ the population of island A or B, γ the relativistic Lorentz factor, $V_{A,B}=(2\pi)^{3/2}\sigma_x\sigma_y\sigma^z_{A,B}$ the bunch volume, σ_x and σ_y the horizontal and vertical rms beam sizes, $\sigma^z_{A,B}$ the rms bunch length in island A or B, $\delta q=\sqrt{\epsilon_x/\beta_x}/(m_0c)$ the uncorrelated horizontal momentum spread, m_0 the electron rest mass, β_x the horizontal beta function, and $\delta^m_{A,B}$ the energy acceptance.

The point on the separatrix which is closest to the stable fixed point $\overline{Q}_B$ can be used to estimate the acceptance of island B. Let us call this point $\overline{Q}_2$. With $\overline{H}_C\equiv\overline{Q}_C/(4\phi_m)^{1/3}$, it reads [3]

$$\overline{Q}_2=(4\phi_m)^{1/3}\left(-\overline{H}_C+\frac{2}{\sqrt{\overline{H}_C}}\right). \tag{12}$$

The island energy acceptance is given by

$$\delta^m_{A,B}\approx\frac{\nu_{s0}}{h\eta}|\overline{Q}_2-\overline{Q}_{A,B}|. \tag{13}$$

Inserting the separatrix energy barrier [Eq. (13)] into the expression for the Touschek loss rate, Eq. (11), and integrating over the nominal Advanced Light Source lattice functions, we finally obtain an estimate of the island-to-island diffusion rate due to Touschek scattering. Figure 8 shows the predicted Touschek diffusion rates as a function of modulation frequency for several beam currents. The strong dependence on the modulation frequency arises since the latter determines the island width and separation, and, thereby, the effective energy acceptance δ^m_B.

Consider a situation where the modulation frequency is slowly swept upward through the resonance. When the modulation frequency begins its sweep well below the bifurcation frequency, only island B is populated. As the modulation frequency slowly increases, islands A and B move closer and island B shrinks. Electrons begin to diffuse from island B to A up to the point where the modulation frequency equals the bifurcation frequency and island B vanishes. Above this point only island A is populated. A similar situation occurs for a downward sweep of the modulation frequency except the electrons start in island A and diffuse to B below the bifurcation frequency. It is interesting to note that it is possible to maintain electrons in island A to larger phase amplitudes by increasing the downward sweep rate above the diffusion rate.

III. MEASUREMENTS

The ALS is a 1.5-GeV electron storage ring optimized for producing high brightness synchrotron radiation. Machine parameters relevant to our experiments are listed in Table I. To make a detailed study of the longitudinal beam dynamics, we used a streak camera (SC) to observe the evolution of the longitudinal bunch distribution as the modulation frequency sweeps both upward and downward through the synchrotron resonance. A schematic diagram of the Hamamatsu C5680 SC is shown in Fig. 3. The SC converts the time structure of a pulse of synchrotron radiation at optical wavelengths from a bend magnet into vertical deflection at the charge-coupled device (CCD) camera. In our experiments, the vertical deflection plates are driven by a 125 MHz sinusoidal voltage synchronized to the rf frequency. In addition, there is an

TABLE I. Nominal ALS parameters.

Parameter	Description	Value
E	Beam energy	1.5 GeV
C	Circumference	196.8 m
f_{rf}	rf frequency	499.658 MHz
h	Harmonic number	328
η	Momentum compaction	1.6×10^{-3}
Q_s	Synchrotron tune	0.0075
λ_{rad}	Long. rad. damping rate	5×10^{-5}
σ_ℓ	rms natural bunch length	4.5 mm
σ_ϵ	rms $\delta E/E$	7.1×10^{-4}
ϵ_x	Norm. hor. emittance	1.2×10^{-5} m

optional slow horizontal deflection which allows observation of the longitudinal profile as a function of time. The time scale of the horizontal sweep can be adjusted to observe a single turn or thousands of turns. For sweep times longer than several hundred turns, individual turns can no longer be resolved, and so the longitudinal profile appears as a continuous line across the image.

Using the SC, we recorded the longitudinal profile as the modulation frequency swept slowly through the resonance. Shown in Fig. 4 are images of the longitudinal profile vs time for three modulation frequencies (f_m): well below the bifurcation frequency, slightly below the bifurcation frequency, and above. The vertical axis is time with respect to a synchronous bunch (i.e., a bunch not executing synchrotron oscillations) where positive displacement indicates early arrival. The horizontal axis represents the relatively slow sweep time of the streak camera. For these images, the horizontal time scale is about 530 turns. The darker area in the image represents higher intensity. The sinusoidal pattern of the distribution is due to the phase modulations (the nominal rms bunch length is 15–20 ps.) At this level of excitation, the bunch has oscillation amplitude of about 100–300 ps peak to peak. Near the bifurcation frequency, the bunch appears to split into two separate beamlets, oscillating with different amplitudes and out of phase by 180°. The charge in the second beamlet increases while the first decreases. Above the bifurcation frequency, the original beamlet disappears and only the second remains. The time at which the second beamlet appears depends on the modulation sweep rate and the bunch current. We observe similar effects for downward sweeps of the modulation frequency, also with dependencies on the sweep rate and bunch current. We verified the simultaneous presence of two beamlets by viewing the profile over only a single turn.

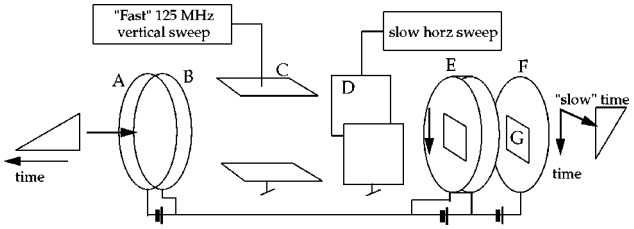

FIG. 3. Schematic diagram of the streak camera in the synchroscan mode with dual sweep. (A) phothcathode, (B) accel. mesh, (C) vert. deflection electrode, (D) horz. defl. electrode, (E) microchannel plate, (F) phosphor screen, and (G) CCD camera.

The modulation amplitude was determined independently by recording the spectrum of a rf cavity probe signal without beam on a spectrum analyzer. The relative amplitude of the phase modulation sidebands to the carrier at the rf frequency accurately determines the amplitude of modulation. The rf cavities were also carefully tuned on resonance to avoid any phase to amplitude modulation conversion.

With the streak camera, we observe the projection of the longitudinal distribution on the horizontal axis in Fig. 2 as the phase space diagram rotates about the origin. When both islands A and B are populated and situated as shown in the phase space diagram, the two beamlets are at their maximum separation in phase (or time). When the phase space has rotated by 90°, the beamlets are coincident in phase but at their maximum energy separation. Figure 4(a) corresponds to the situation where there are two stable islands but only island B is populated. In Fig. 4(b), the modulation frequency has increased, and islands $A$and B are populated but oscillating at different amplitudes. In Fig. 4(c), the modulation frequency is above the bifurcation frequency and only island A exists.

From this, the stable fixed points can be measured as a function of modulation frequency by simply measuring the amplitudes of the sinusoidal curves in Fig. 4 as long as they contain charge. Shown in Fig. 5 are the response curves for upward and downward sweeps of the modulation frequency along with the calculated response curves. The upward and downward sweep measurements were made at different times with somewhat different parameters. Note that the downward sweep allows measurement of the response to larger amplitudes on the upper branch of the response curve. The measured fixed points show good agreement with the calculated values for the applied modulation amplitude.

A. Interisland diffusion

To measure the diffusion rates, we filled a single bunch with current, and used the SC to measure the longitudinal profile as a function of time after initiating the phase modulation at a fixed frequency. The modulation frequency was always below the bifurcation frequency, ensuring the presence of two stable islands. For each beam current, we measured the diffusion as a function of modulation frequency in order to vary the island size and separation. In order to improve the observable signal level in the outer island A, we used the SC without horizontal sweeping. In this mode, we observe the longitudinal profile averaged over a video cycle. This is roughly equivalent to taking the vertical projection of the images in Fig. 4, but over a longer time period.

An example demonstrating the diffusion from island B to island A is shown in Figs. 6(a) and 6(b). Figure 6(a) shows an example of the longitudinal profile averaged over about 200 synchrotron oscillations. This profile was obtained about 85 s after initiating the phase modulation with a 1-mA bunch current. The charge in island A appears as the ''wings'' of the profile, and the charge in the island B appears as the two central peaks. Figure 6(b) consists of a sequence of profiles obtained at 2-s intervals combined together to form an image of the diffusion. The increase of charge in island A as a function of time is evident, as well as a small decrease in the island B. Eventually the population in both islands reaches an equilibrium.

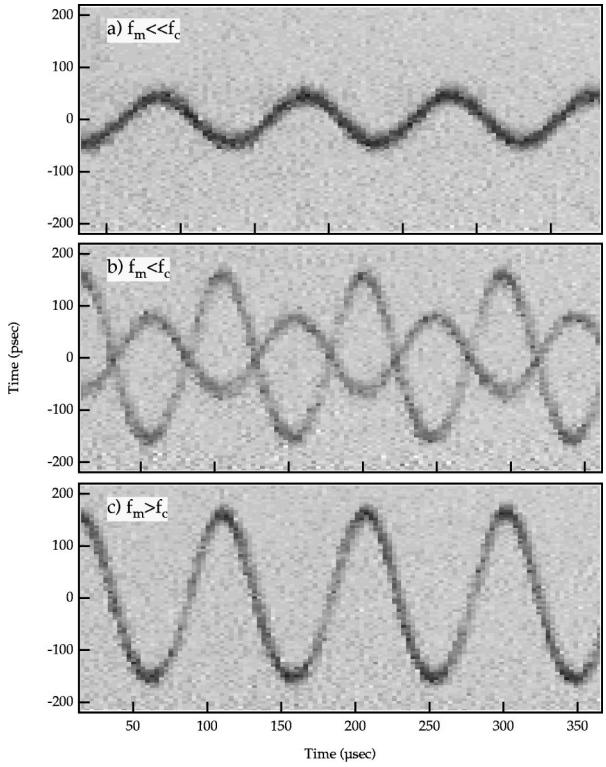

FIG. 4. Images of the longitudinal profile (in ps) vs time using the streak camera in the dual scan mode: (a) f_m well below the bifurcation frequency; (b) f_m just below the bifurcation frequency; (c) f_m above the bifurcation frequency.

We extracted the initial diffusion rate by comparing the relative rate of increase of the peak signal in island A(outer island) compared to island B (central island.) The diffusion for the case of a modulation frequency of 11.069 kHz is shown in Fig. 7. A plot of the diffusion rates as a function of modulation frequency for several beam currents is shown in Fig. 8.

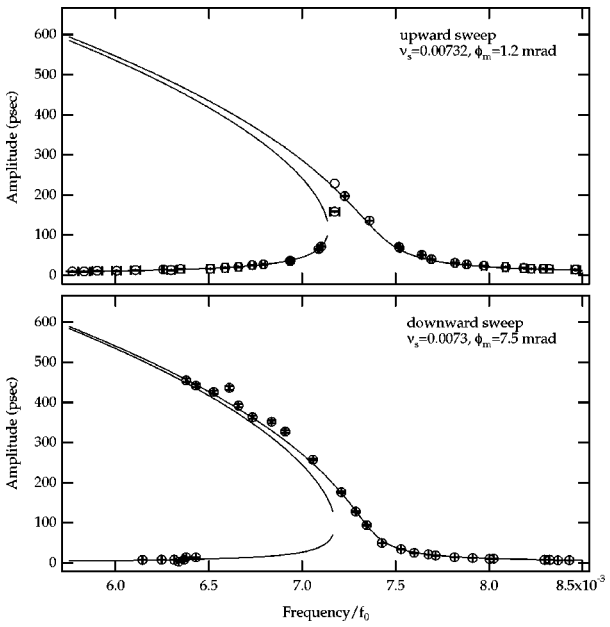

FIG. 5. Measured response curve for a modulation frequency swept upwards and downwards through the resonance.

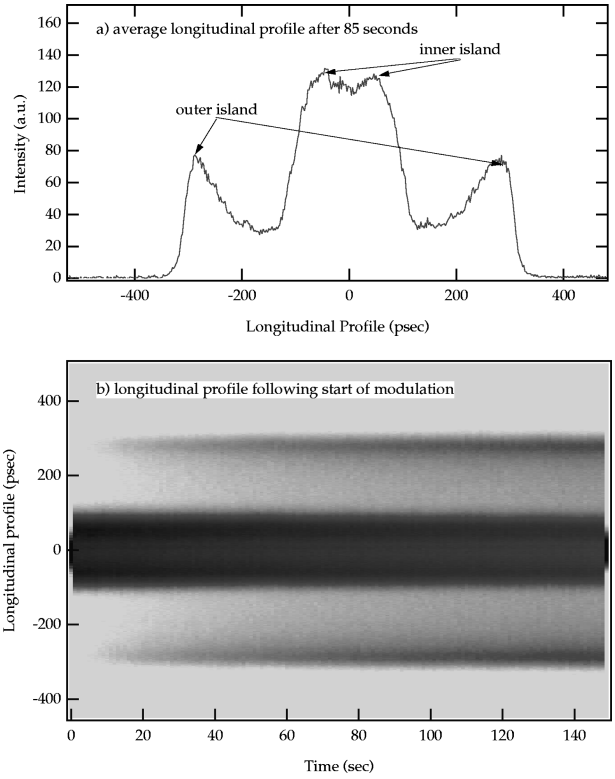

FIG. 6. (a) Time-averaged longitudinal profile about 85 s after the starting modulation. The central peaks correspond to the central island and the outer peaks to the outer island. (b) Longitudinal profile vs time, showing diffusion from the inner island to the outer island.

The agreement with the calculated diffusion rates is good, considering the degree of approximation in the calculation. The betatron coupling value of 1.5% used in the calculation of the diffusion rate was estimated from the ratio of measured vertical to horizontal beam size using a synchrotron radiation image of the transverse beam profile at a point with known β functions.

B. Beam transfer function measurements

Beam transfer function (BTF) techniques are common in accelerators. In its simplest form, a swept frequency drive is used to excite beam oscillations in order to measure the syn-

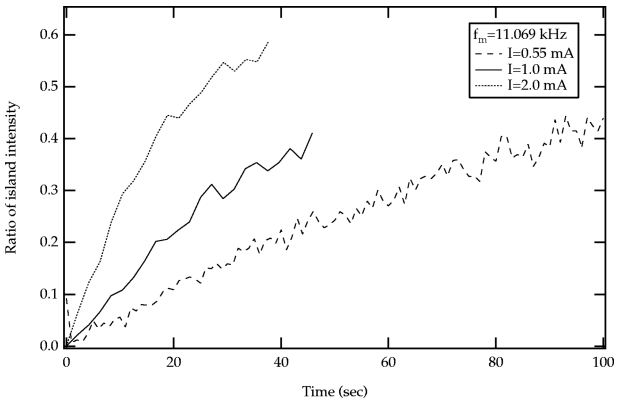

FIG. 7. Peak intensity of the outer island normalized to the inner island as a function of time for a modulation frequency of 11.069 kHz.

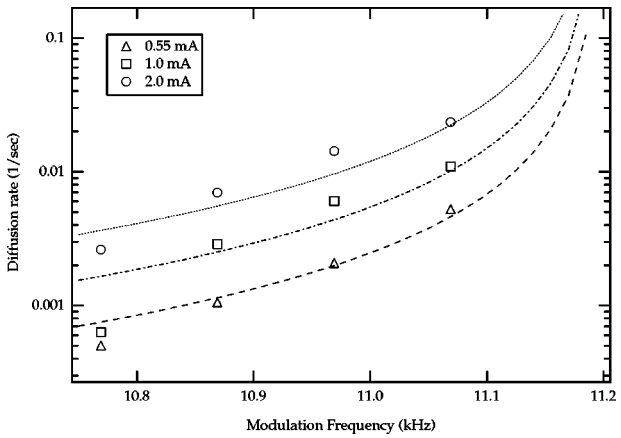

FIG. 8. Measured and predicted diffusion rates as a function of modulation frequency for three different bunch currents.

chrotron or betatron tunes. The BTF can also be used to measure the beam impedance and various other machine parameters [10–13]. In the course of BTF measurements at the ALS, we observed an unusual phenomenon in the longitudinal transfer function. As the level of excitation was increased, a deep notch appeared in the amplitude response of the BTF. Similar observations were made at the Stanford Linear Collider electron damping ring [14] and the Cornell Electron Storage Ring [15]. In this section we present an explanation of this anomalous effect in terms of the nonlinear discussed previously.

Our setup for measurement of the BTF at the ALS is shown in Fig. 9. We excited longitudinal oscillations by phase modulating the rf voltage. This was achieved by injecting the modulation signal as an error signal in the rf phase control feedback loop. Synchrotron oscillations were detected by comparing the phase of a beam pickup signal relative to a fixed reference phase using an existing phase detector for the longitudinal coupled-bunch feedback system [7]. This detector passes the sum of the signal from four capacitive button beam position monitors located at one point in the ring through a four-tap comb filter with a center frequency of 3 GHz ($6f_{\mathrm{rf}}$). The sum of the four button signals is not sensitive to the transverse position of the beam. The signal is demodulated to baseband through a double balanced mixer using a 3-GHz local oscillator derived from the 500-MHz master oscillator. Detection at the sixth rf harmonic increases the sensitivity to phase oscillations compared to detection at the rf frequency and is also near the frequency of maximum pickup impedance of the BPM's. For the measurements in this paper, the amplitude of synchrotron oscillations is kept within the linear range of the detector.

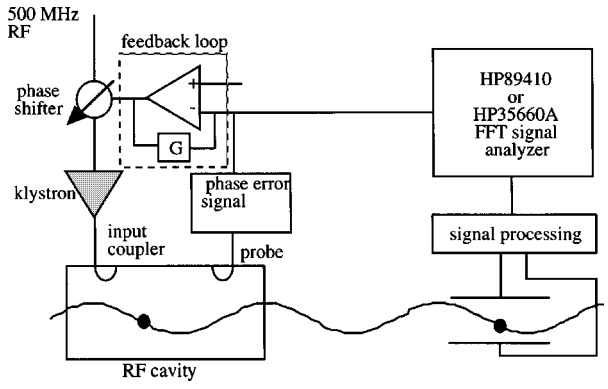

FIG. 9. General setup for longitudinal BTF measurements.

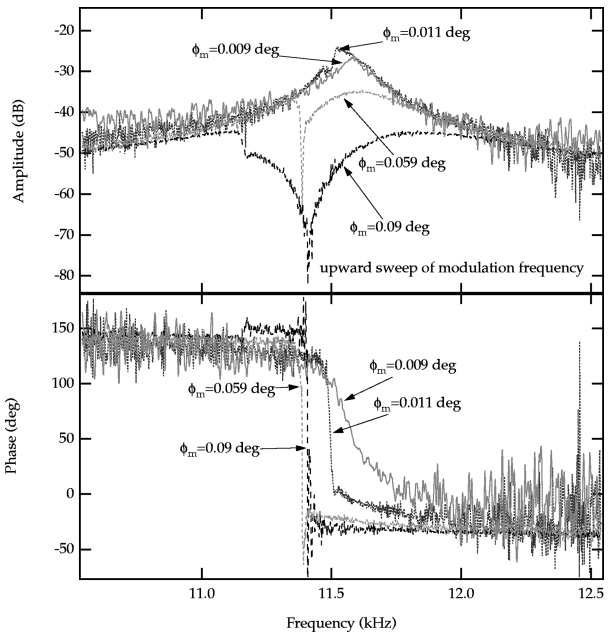

FIG. 10. Amplitude and phase of the longitudinal beam transfer function for various drive amplitudes for an upward sweep of the modulation frequency.

Shown in Figs. 10 and 11 are plots of the amplitude and phase of single bunch longitudinal BTF measurements as a function of modulation frequency for different amplitudes of phase modulation. In Fig. 10, the excitation frequency was swept from lower to higher frequency, and in Fig. 11 the frequency was swept in the opposite direction. In the first

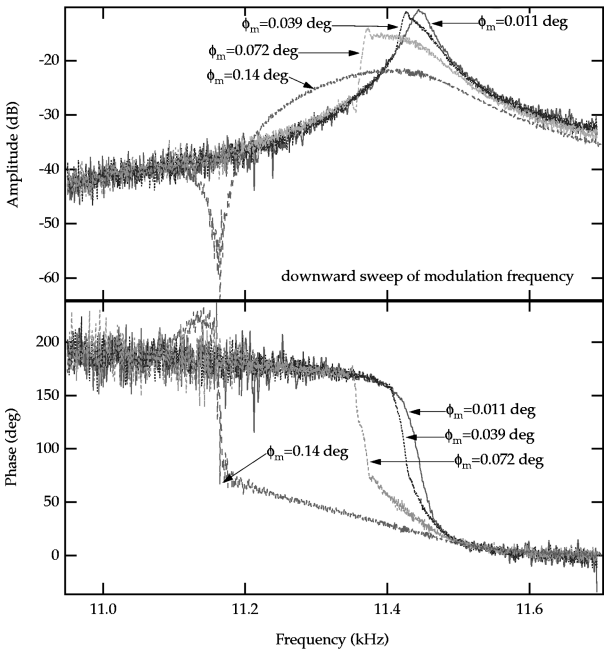

FIG. 11. Amplitude and phase of the longitudinal beam transfer function for various drive amplitudes for a downward sweep of the modulation frequency.

case, the time to sweep the frequency across the span was 100 s. For the downward swept case shown, the sweep time was about 10 s. The bunch current in both cases was 0.5 mA.

At small excitation amplitudes, the BTF agrees with expectation [13] for both upward and downward swept excitations. However, the BTF exhibited a severe distortion as the excitation was increased, as demonstrated by the deep notch and sudden 180° phase shifts in both the amplitude and phase for both upward and downward frequency sweeps. Another feature not shown here is the strong dependence of the notch frequency on the sweep direction, the sweep rate, the bunch current, and the nominal synchrotron frequency.

From the streak camera data shown in Fig. 4, an explanation for the notch and the sudden 180° phase shift in the BTF data presents itself. The phase detector for the BTF is sensitive only to *net* dipole phase oscillations of the bunch. As the modulation frequency approaches the bifurcation frequency, charge diffuses from island B to island A because of Touschek scattering. In the lab coordinate frame, island B oscillates out of phase with island A. At some frequency, enough charge has diffused from the first beamlet to the second such that the dipole moments of the two cancel. At this frequency, a notch appears in the BTF. The 180° phase shift in the BTF occurs because of the relative phase of the two beamlets.

From the analysis above, we believe that the effect observed in the BTF is universal for longitudinal beam response measurements in storage rings, including hadron rings. The precise behavior is a function of the ring parameters, the diffusion rate, and the sweep rate. This may prove to be a useful tool for measuring the diffusion rate without the aid of a more sophisticated equipment such as a streak camera.

IV. DISCUSSION AND CONCLUSIONS

Nonlinearity of the synchrotron oscillations in the presence of phase modulation can have a dramatic effect on the behavior of the longitudinal charge distribution of an electron bunch in the presence of phase modulation. The nonlinearity allows for the formation of multiple ''beamlets'' within a rf bucket. The dominant diffusion mechanism between beamlets for the conditions at the ALS is large-angle intrabeam scattering, although we expect that at very low beam currents the diffusion from quantum excitation might be observable. Anomalous effects in longitudinal BTF measurements observed at the ALS and at other storage rings can be explained in terms of the multiple beamlets formed in the rf bucket.

It is clear that this phenomenon has an impact on the growth and saturation of coherent beam instabilities. For example, in a coherent multibunch instability, the electron bunches should bifurcate into multiple ''beamlets'' as the oscillation amplitude increases. When the net dipole moment is cancelled, as in the case of the BTF, the driving mechanism for the instability vanishes and the growth begins to damp. The nonlinearity may be responsible for a beating phenomenon that results in slow periodic fluctuations in average bunch length that has been observed in many storage rings in multibunch operation. The creation of stable fixed points at large amplitude also opens the possibility of exotic resonant injection or extraction schemes. For example, by rapidly sweeping the modulation frequency downwards through the synchrotron resonance, we can transport some fraction of the beam to large energy offset which can be extracted in a dispersive region. We hope that the methods discussed here can be extended further to be useful in studies of topics such as higher order momentum compaction, collective effects, and Touschek and intrabeam scattering.

ACKNOWLEDGMENTS

We would like to thank the ALS operations group for assistance in doing the measurements. This work was supported by the U.S. Department of Energy under Contract Nos. DE-AC03-76SF00098, DE-FG-03-95ER40936, and DE-AC03-76SF00515.

[1] S. A. Heifets, Phys. Rev. E **54**, 2889 (1996).
[2] J. M. Byrd and J. Corlett, Part. Accel. **51**, 29 (1995).
[3] M. Ellison *et al.*, Phys. Rev. Lett. **70**, 591 (1993).
[4] H. Huang *et al.*, Phys. Rev. E **48**, 4678 (1993).
[5] D. Li *et al.*, Phys. Rev. E **48**, 1638 (1993).
[6] D. Li *et al.*, Nucl. Instrum. Methods Phys. Res. Sect. A **361**, 205 (1995).
[7] J. D. Fox *et al.*, in *Proceedings of the 1996 European Particle Accelerator Conference*, edited by S. Myers (IPP, Philadelphia, 1997), p. 346.
[8] H. Bruck, *Accelerateurs Circulaires de Particules* (Presses Université, Paris, 1966).
[9] R. P. Walker, in *Proceedings of the 1987 IEEE Particle Accelerator Conference*, edited by E. Lindstrom, Washington, D.C. (IEEE, New York, 1988), p. 491.
[10] A. Hofmann and B. Zotter, in *Proceedings of the 1977 IEEE Particle Accelerator Conference*, edited by F. Coles, Chicago, IL (IEEE, New York, 1978), p. 1487.
[11] J. M. Jowett *et al.*, in *Proceedings of the 1987 IEEE Particle Accelerator Conference* (Ref. [9]), p. 726.
[12] A. Hofmann, in *Proceedings of 1987 CERN Accelerator School*, edited by S. Turner, CERN Report No. 89-01 (CERN, Geneva, 1989), p. 40.
[13] J. M. Byrd, Part. Accel. **57**, 159 (1997).
[14] M. Minty and F. Zimmermann, in *Proceedings of the 1997 IEEE Particle Accelerator Conference, Vancouver, B.C.* (unpublished).
[15] D. Rice (private communication).